THE JOURNAL OF BIOLOGICAL CHEMISTRY
Vol. 277, No. 40, Issue of October 4, pp. 37597–37603, 2002

The Solution Structure of Human Hepcidin, a Peptide Hormone with Antimicrobial Activity That Is Involved in Iron Uptake and Hereditary Hemochromatosis*[S]

Received for publication, May 29, 2002, and in revised form, July 19, 2002
Published, JBC Papers in Press, July 22, 2002, DOI 10.1074/jbc.M205305200

Howard N. Hunter‡, D. Bruce Fulton§, Tomas Ganz¶, and Hans J. Vogel‡‖

From the ‡Department of Biological Sciences, University of Calgary, Calgary, Alberta T2N 1N4, Canada, §Department of Biochemistry, Biophysics and Molecular Biology, Iowa State University, Ames, Iowa 50011-3260, and ¶Departments of Medicine and Pathology, UCLA School of Medicine, Los Angeles, California 90059

The antibacterial and antifungal peptide hepcidin (LEAP-1) is expressed in the liver. This circulating peptide has recently been found to also act as a signaling molecule in iron metabolism. As such, it plays an important role in hereditary hemochromatosis, a serious iron overload disease. In this study, we report the solution structures of the hepcidin-20 and -25 amino acid peptides determined by standard two-dimensional ^{1}H NMR spectroscopy. These small cysteine-rich peptides form a distorted β-sheet with an unusual vicinal disulfide bridge found at the turn of the hairpin, which is probably of functional significance. Both peptides exhibit an overall amphipathic structure with six of the eight Cys involved in maintaining interstrand connectivity. Hepcidin-25 assumes major and minor conformations centered about the Pro residue near the N-terminal end. Further NMR diffusion studies indicate that hepcidin-20 exists as a monomer in solution, whereas hepcidin-25 readily aggregates, a property that may contribute to the different activities of the two peptides. The nuclear Overhauser enhancement spectroscopy spectra of the hepcidin-25 aggregates indicate an interface for peptide interactions that again involves the first five residues from the N-terminal end.

Hepcidin is a cysteine-rich cationic peptide that was recently isolated from human urine (1) and plasma ultrafiltrate (2) and was found to have antibacterial and antifungal activity. Human urine contains two predominant forms, comprised of 20 and 25 amino acids each, that differ only by N-terminal truncation. The 84-amino acid hepcidin prepropeptide contains a typical endoplasmic reticulum targeting signal sequence and a consensus cleavage site for prohormone convertases. In humans, the prepropeptide is encoded by a single gene whose major site of expression is the liver (1–3). Although close hepcidin homologues have been identified in vertebrates ranging from fish to mammals (4), hepcidin does not appear to be related to any other previously known peptide family.

Independently, hepcidin mRNA was found to be induced in the livers of mice by iron overload or treatment with lipopolysaccharide (3). The likely role of hepcidin in iron metabolism was further suggested by the observation that mice with disruption of the gene encoding the transcription factor USF2 failed to produce hepcidin mRNA and developed spontaneous visceral iron overload (5). Because the USF2 gene is located immediately upstream of the two murine hepcidin genes, and its disruption by *neo* gene insertion exerts a detectable effect even in a heterozygous state, it is thought that the upstream *neo* insertion exerts a *cis*-inhibitory effect on the downstream genes. In contrast, mice engineered to overexpress hepcidin experience severe iron deficiency anemia (6). Based on these observations, it has been suggested that hepcidin is the long-sought signaling molecule that decreases iron absorption in the small intestine and iron release from stores in macrophages (7), in response to increased visceral iron stores or inflammation. The increase of hepcidin by inflammatory stimuli could serve the host defense strategy of denying essential iron to infecting microbes.

Analysis of the sequence of hepcidin (DTHFPICIFCCGCCHRSKCGMCCKT) revealed a very high percentage of cysteines (eight cysteines in both the 20- and 25-residue peptide). This is an unusually high amount of Cys when compared with the composition of other cysteine-rich antimicrobial peptides such as the defensins (8), tachyplesin (9), protegrin (10), and, more recently, snakin (11). Mass spectroscopy and chemical analysis have revealed that all of the Cys are bridged in the sequence, making this peptide a highly constrained peptide (1). The use of CD spectroscopy in the same study indicated the presence of a loop and a distorted β-sheet. Furthermore, hepcidin-20 was found to be generally more active against *Staphylococcus aureus*, *Staphylococcus epidermis,* group B *Streptococcus*, and *Candida albicans*.

Clearly, a complete three-dimensional structural elucidation could give insight into the recognition of this peptide in both an antimicrobial and iron-regulatory capacity. Here we present an investigation of the structure and a study of the aggregation properties observed from ^{1}H NMR spectroscopy to show the amphipathic character as well as the unique structural characteristics of the 20- and 25-amino acid peptides (hepcidin-20 and hepcidin-25, respectively).

EXPERIMENTAL PROCEDURES

Materials—D_2O 99.9% was purchased from Cambridge Isotope Laboratories, Inc. (Andover, MA). Gold label D_2O and dioxane were purchased from Aldrich.

Peptide Synthesis and Refolding—Peptide synthesis was completed exactly as described previously (1). For the 25-residue peptide, isotopi-

* This work was supported by an operating grant from the Canadian Institute for Health Research (to H. J. V.). The costs of publication of this article were defrayed in part by the payment of page charges. This article must therefore be hereby marked "*advertisement*" in accordance with 18 U.S.C. Section 1734 solely to indicate this fact.

[S] The on-line version of this article (available at http://www.jbc.org) contains Figs. 1S–3S.

The atomic coordinates and structure factors (code 1M4E and 1M4F) have been deposited in the Protein Data Bank, Research Collaboratory for Structural Bioinformatics, Rutgers University, New Brunswick, NJ (http://www.rcsb.org/).

‖ Holds a Scientist Award from the Alberta Heritage Foundation for Medical Research. To whom correspondence should be addressed. Tel.: 403-220-6006; Fax: 403-289-9311; E-mail: vogel@ucalgary.ca.

cally labeled amino acids ^{15}N-Ile, ^{15}N-Phe, and ^{15}N-Gly were used in the Fmoc (*N*-(9-fluorenyl)methoxycarbonyl) process. Both isotopic forms of the refolded synthetic hepcidin had the predicted masses by spectrometry, and, when compared with the natural hepcidin (20- and 25-amino acid forms) isolated from urine (1), migrated identically in 12.5% acid-urea PAGE and had an identical retention time on C18 reverse phase high precision liquid chromatography.

NMR Spectroscopy—Approximately 2 mg of the 20-amino acid peptide was dissolved in 550 μl of 90:10 H_2O:D_2O. The unadjusted pH was 3.2, and the concentration was determined to be 0.783 mM using UV absorption at 280 nm and a calculated molar extinction coefficient based on the number of half Cys residues in the peptide (480 M^{-1} cm^{-1}).

The NMR sample of the 25-residue peptide was prepared by dissolving 6.8 mg of purified peptide in 0.5 ml of 40 mM phosphate buffer, pH 3.5 (90% H_2O:10% D_2O). The concentration of the original aqueous sample was determined to be 1.6×10^{-3} M using UV absorption at 280 nm.

To determine the NMR structure of both the 20- and 25-amino acid peptides, various NMR field strengths were used. The two-dimensional NOESY[1] (mixing times of 200 ms) and TOCSY (mixing times of 120 ms) spectra were acquired at 25 °C on Bruker DRX 500 MHz and DRX 700 MHz NMR spectrometers. A separate NOESY spectrum was acquired at 13 °C at 500 MHz. The same experiments were acquired with the D_2O sample using the INOVA 800 MHz spectrometer at the National High Field Nuclear Magnetic Resonance Centre (University of Alberta, Edmonton, Alberta, Canada). The two-dimensional NOESY and two-dimensional TOCSY experiments were also repeated at 400 MHz without ^{15}N decoupling. All two-dimensional experiments for the 25-amino acid peptide were ^{15}N decoupled during evolution and acquisition periods. A series of NOESY spectra were also collected over a range of mixing times of 50, 100, 150, 200, 300, 400, 500, and 600 ms for the two samples to monitor the NOE buildup. The spectra were acquired at 500 MHz with 2048 $\times$ 600 data points in the directly and indirectly detected dimensions, respectively, and spectral widths of 6009 Hz. The 700 MHz spectra were acquired with 2048 $\times$ 600 data points with 80 scans/increment. At 800 MHz, the data were collected with 2048 $\times$ 600 data points in the directly and indirectly detected dimensions, respectively, and spectral widths of 6009 Hz. Water suppression was achieved using excitation sculpting (12).

The two-dimensional TOCSY and NOESY NMR spectra were processed with NMRPipe 3.4 and analyzed with the NMRView 4.1.3 (13) software package on workstations operating with the Redhat 7.1 version of the Linux operating system. The two-dimensional data were zero-filled once in each dimension and Fourier-transformed with a shifted sine-bell squared function. All NMR spectra were referenced externally to sodium 3-(trimethylsilyl)-1-propanesulfonate at 0.0 ppm.

To determine which amides were in slow exchange, the sample was dissolved in D_2O. Immediately after dissolution, a series of one-dimensional ^{1}H spectra were acquired over the following 24 h. Twenty min after the first ^{1}H spectrum was acquired, a 1-h two-dimensional TOCSY spectrum was collected.

A ^{1}H-^{13}C heteronuclear single quantum coherence experiment was acquired at 700 MHz for hepcidin-20 with 1024 $\times$ 128 data points over spectral widths of 9765 $\times$ 4401 Hz and referenced to internal dioxane. A ^{1}H-^{15}N heteronuclear single quantum coherence was acquired at 500 MHz using hepcidin-25 to confirm the identity of the ^{15}N-labeled amino acids.

NMR Diffusion—For the NMR diffusion experiments, each sample was dissolved in D_2O, and peptide diffusion was monitored relative to internal dioxane (14, 15).[2] Approximately 5 μl of a 1% solution of dioxane in D_2O was added to the sample as an internal standard. Pulsed field gradient diffusion experiments were collected with the PG-SLED sequence (16). The data were acquired at 700 MHz for hepcidin-20 and 400 MHz for hepcidin-25 using NMR probeheads equipped with proton observe and 3-axis gradient coils. Samples of peptide were dissolved in 100 μl of D_2O in a Shigemi tube (Shigemi Co., Ltd., Tokyo, Japan). The data were acquired by collecting 56 scans of 16,000 data points at each gradient amplitude and incrementing the gradient strength in 64 steps from 1.25% to 80% of the maximum output of the linear gradient amplifier. After data collection was completed, hepcidin-25 was diluted with 100 μl of D_2O, and data were reacquired. To process the data, a 1 Hz line broadening value was applied before Fourier transformation with the Bruker XWINNMR package version 2.6 at 400 MHz and version 3.0 at 700 MHz. From the resulting series of spectra, not fewer than 5 peptide resonances were chosen, and the decay of the peak intensities as a function of gradient strength was evaluated using the XWINNMR package. The one-dimensional spectra of the 20-amino acid peptide indicated that no spectral overlap occurred between the dioxane resonance and the peptide. However, the dioxane signal overlapped with a portion of the 25-amino acid peptide. Therefore, an average of the five peptide diffusion rates was used to fit the decay of the reference dioxane peak to a biexponential function. Calculated values for the hydrodynamic radii were determined using the previously determined empirical relationship (14).

Structure Calculation—The assignment of the protein chemical shifts was determined using standard methods. Upon completion of the proton assignments, NOE-based distance restraints were collected from NOESY spectra and automatically allocated to close, medium range, and long distance interactions based upon intensity. A broad dihedral angle restraint was used to confine the bond angles (except for Gly) to the allowed Ramachandran space. The protein structures were determined using the programs CNS 1.1 (17) and ARIA (18). ARIA calculations were initiated using default parameters. In the final ARIA run, the number of structures generated in the seventh and eighth iterations was increased to 40 and 100, and in the eighth iteration, the 20 lowest energy structures were used for statistical analyses. For hepcidin-20, restraints were used from two-dimensional NOESY spectra at mixing times of 200, 400, and 600 ms at 700 MHz; 400 ms at 500 MHz; and 400 ms in D_2O solution at 400 MHz. For hepcidin-25, constraints were used from the two-dimensional NOESY spectrum collected with a mixing time of 150 ms at 800 MHz. Molecular structures were viewed using MOLMOL (19) or GRASP (20) and analyzed using PROCHECK (21).

Sedimentation Equilibrium Analyses—Samples were dialyzed against 100 mM NaCl and 50 mM citrate buffer at pH 3.5. Data were obtained at 20 °C using a Beckman XL-I ultracentrifuge equipped with absorbance optics using spinning speeds of 26,000, 32,000, 38,000, and 44,000 rpm.

Light Scattering—Dynamic light scattering experiments were obtained at 25 °C with a DynaPro MSTC light scattering instrument (Protein Solutions Inc., Lakewood, NJ) using a laser wavelength of 827.6 nm. Before data acquisition, both a blank and 0.783 μM hepcidin-20 peptide sample were filtered through 0.02 mm Anodisc 13 (Whatman International Ltd., Maidstone, United Kingdom) filters. For each sample, 100 data points were collected, and the hydrodynamic radii of the prominent species were evaluated using the Stokes-Einstein equation included in the Dynamics software (version 6.1.06).

RESULTS AND DISCUSSION

Nomenclature—To simplify the numbering, the cysteine residues will be referred to by their position in each peptide (*i.e.* first, second, third, and so forth), with numbering beginning at the N-terminal end of the peptide.

Spectral Assignment and Structure Calculation for Hepcidin-20—The shorter of the two peptides proved to be the more straightforward to assign because of good dispersion and well-resolved peaks in the NMR spectra. Using standard methods, near complete proton assignments were obtained. The amide proton resonances for the fourth and fifth Cys residues could not be observed in the two-dimensional TOCSY at room temperature or at lower temperatures for this peptide. Only at 500 MHz could very broad low intensity correlations be observed between the αH and β-protons of these two residues. The inability to resolve the two amide resonances is consistent with an exchange process occurring on the NMR time scale involving the fourth and fifth cysteine residues. In the two-dimensional TOCSY spectrum, there were two slightly offset amide correlations observed for the Thr^{20} residue, consistent with two separate conformations for this C-terminal amino acid. There were several α-protons with chemical shifts consistent with β-sheet structure. To fully evaluate the chemical shift analysis using chemical shift index, a ^{1}H-^{13}C heteronuclear single quantum coherence experiment was acquired. The α-^{13}C chemical shift values (22) (except for the fourth and fifth cysteine α-^{13}C resonances that were not detected) are shown in Fig. 1*B*. The

[1] The abbreviations used are: NOESY, nuclear Overhauser enhancement spectroscopy; NOE, nuclear Overhauser enhancement; TOCSY, total correlation spectroscopy.

[2] A. M. Weljie, H. Yoshino, A. P. Yamniuk, and H. J. Vogel, manuscript in preparation.

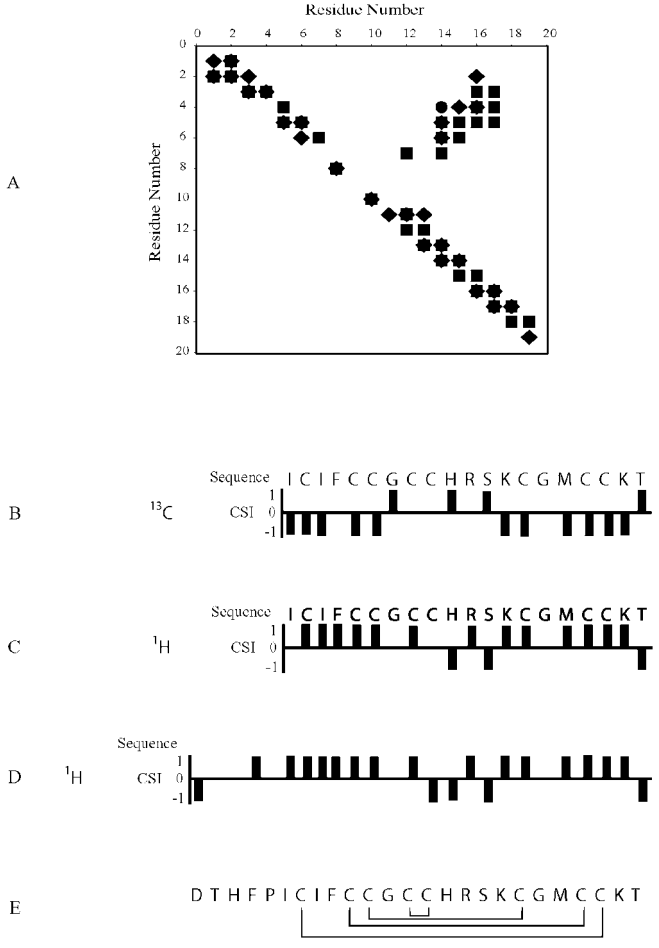

FIG. 1. *A*, contact plot indicating backbone-backbone (■), backbone-side chain (◆), and side chain-side chain (●) unambiguous NOE interactions. The off-diagonal interactions represent 22 NOE interactions for a distance of >4 sequential residues. The chemical shift index plots are shown for hepcidin-20 ^{13}C (*B*) and proton (*C*) chemical shifts and hepcidin-25 proton shifts (*D*). The hepcidin-25 sequence is shown with the disulfide connectivity in *E*.

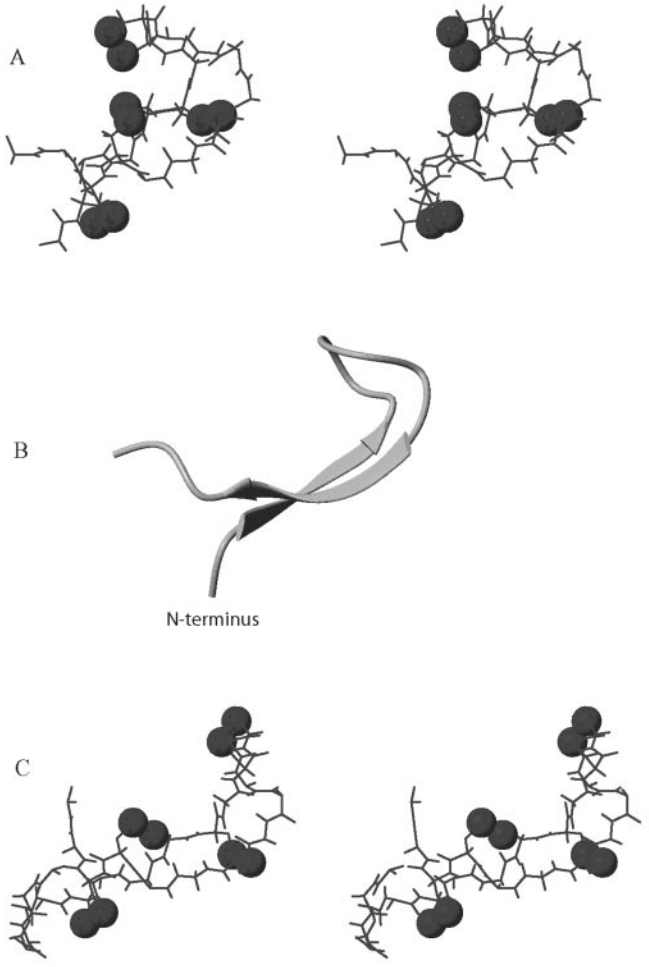

FIG. 2. Stereoviews of the lowest energy calculated structures of hepcidin-20 (*A*) and hepcidin-25 (*C*), with sulfur atoms shown as *large spheres*. The ribbon diagram corresponding to hepcidin-20 is shown in *B*. All structures were generated with MOLMOL.

evaluation of the α-proton chemical shifts using the chemical shift index (23) is shown in Fig. 1*C*. Together, the indices show β-sheet character for significant portions of this peptide.

A previous study confirmed that all eight Cys residues formed intramolecular bonds, but the identity of the pairings between individual Cys residues could not be determined (1). Consequently, results from every NMR experiment were carefully examined to help elucidate the location of the four disulfide bridges. The NOE interactions indicated that the N- and C-terminal ends of the peptide sequence were interacting. Therefore, the initial structural calculation using ARIA contained only the few NOE constraints along with sequential constraints provided by a single two-dimensional NOESY spectrum without assigned disulfide linkages or hydrogen bond assignments (24). The lowest energy structures obtained from these calculations assisted in the determination of the identity of the other ambiguous assignments. As more constraints were identified, it became obvious that two of the disulfide linkages were between the first and eighth Cys and the third and sixth Cys residues (Fig. 1*E*). The first and eighth Cys showed strong αH-αH and αH-βH interactions, whereas the third and sixth Cys amino acids showed an interaction between αH and βH protons from these two cysteines. Additional constraints for ARIA calculations came from backbone amide NH-αH dihedral J-coupling values measured from the amide protons in the fingerprint region of the two-dimensional TOCSY experiment.

Whereas the NOE evidence alone did not allow for decisive assignment of the remaining two disulfide bonds, several other independent observations demonstrate the second to seventh and fourth to fifth disulfide pairings.

Results from the D_2O exchange experiments indicated that the five backbone amide protons which were slow to exchange were Ile^3, Phe^4, Cys^5, Gly^{15}, and Cys^{17}. Introducing the three possible pairings for the two disulfide bonds into the ARIA calculation produced structures in which the Ile^3 and Cys^{17} amide protons could establish an antiparallel cross-strand interaction by the formation of hydrogen bonds with the carbonyl oxygens of these two opposing residues. Likewise a similar double hydrogen bond between Cys^5 and Gly^{15} could easily be seen in the resulting structures. Therefore, these four hydrogen bond restraints were introduced, and the structures were recalculated. However, these additional hydrogen bond constraints did not reduce the overall energy difference between the three remaining possible disulfide interactions. Although a rough sketch of the emerging β-sheet pattern would lead to the conclusion that the second and seventh and the fourth and fifth cysteines would be the reasonable choices for the formation of disulfide bonds, visual comparison of the three possible structures indicated that the peptide could easily alter conformation to form one of the other two puckered shapes.

Several independent observations supported a structure bridging the second to seventh and fourth to fifth Cys residues.

TABLE I
Structural statistics for the final 20 structures of hepcidin-20 and -25

	Hepcidin-20	Hepcidin-25
No. of distance restraints		
Unambiguous NOEs	276	242
Ambiguous NOEs	9	9
Total NOEs	285	251
No. of dihedral restraints	17	22
Root mean square distances from ideal values		
Bonds (Å)	$4.96 \times 10^{-3} \pm 1.16 \times 10^{-4}$	$4.59 \times 10^{-3} \pm 2.18 \times 10^{-4}$
Angles (degree)	$0.545 \pm 1.30 \times 10^{-2}$	$0.586 \pm 4.57 \times 10^{-2}$
Impropers (degree)	$0.576 \pm 3.46 \times 10^{-2}$	$0.658 \pm 8.88 \times 10^{-2}$
van der Waals (kcal/mol)	18.07 ± 2.15	26.72 ± 2.25
Distance restraints		
Unambiguous (Å)	$2.66 \times 10^{-2} \pm 1.47 \times 10^{-2}$	$1.97 \times 10^{-2} \pm 4.32 \times 10^{-2}$
Ambiguous (Å)	$6.07 \times 10^{-3} \pm 1.82 \times 10^{-2}$	$1.99 \times 10^{-2} \pm 1.59 \times 10^{-2}$
All distance restraints (Å)	$2.74 \times 10^{-2} \pm 1.34 \times 10^{-2}$	$1.99 \times 10^{-2} \pm 4.68 \times 10^{-3}$
Dihedral restraints (degree)	1.00 ± 0.16	1.06 ± 0.25
Nonbonded energies		
Electronic (kcal/mol)	-411.24 ± 97.66	-485.06 ± 203.02
van der Waals (kcal/mol)	-102.02 ± 23.60	-114.56 ± 46.94
Ramachandran (%)[a]		
Most favored	50.0	70.0
Additionally allowed	43.8	25.0
Generously allowed	6.2	5.0
Disallowed	0.0	0.0
Global root mean square distance (Å)[b]		
	2–19 + bb 0.696	2–24 + bb 1.68
	2–19 + heavy 1.530	2–24 + heavy 2.51
	2–7, 12–19 + bb 0.524	5–12, 17–23 + bb 1.24
	2–7, 12–19 + heavy 1.182	5–12, 17–23 + heavy 1.71

[a] Determined by PROCHECK. ϕ/ψ angles were restrained to allowed values (see "Experimental Procedures").
[b] Calculated using MOLMOL.

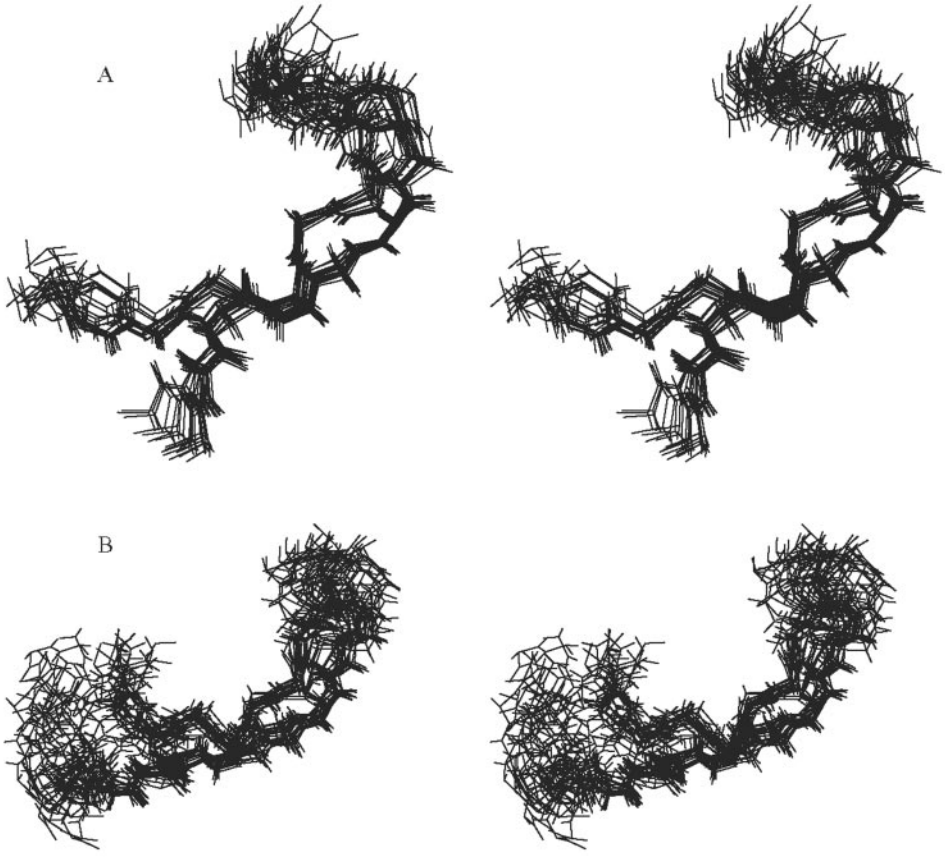

FIG. 3. **Stereoviews of the backbone atoms for the 20 lowest energy structures for hepcidin-20 (*A*) and hepcidin-25 (*B*).**

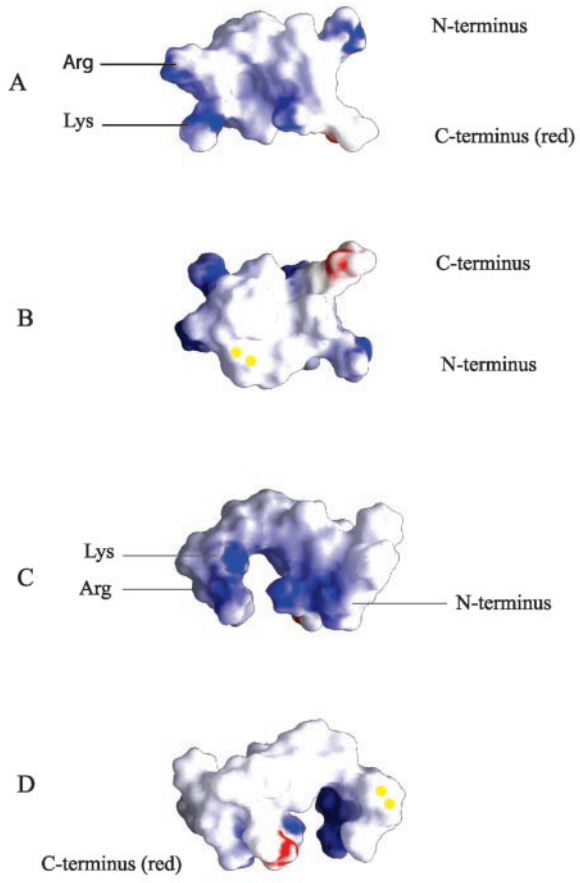

FIG. 4. **Two views of space-filling diagrams of hepcidin-20 (*A* and *B*) and hepcidin-25 (*C* and *D*) indicating cationic charges (*blue*) on *A* and *C* and hydrophobic (*white*) side with vicinal disulfide (*yellow*) on *B* and *D*.** Structures were generated with GRASP.

Assignment of the TOCSY and NOESY spectra from all of the various field strengths and conditions indicated the absence of the backbone amide proton correlations in the fingerprint region only for the fourth and fifth Cys residues. In addition, the broad correlations for the α- and β-protons indicated that exchange is occurring with these two residues on the NMR time scale. The formation of a vicinal cysteine disulfide bridge would result in the formation of an eight-member ring that would be fluxionally mobile. This unusual connectivity, although rare, is not unique in naturally occurring systems (25). The other two possible bridges would link either the second and fourth or the second and fifth Cys residues together. Given the broad line shape of the amide, α- and β-protons for the fourth and fifth cysteines, it would be expected that the cysteines involved with the other half of the disulfide bridge would also show indications of resonance broadening caused by chemical exchange if bonded to the other cysteines. The broadening of these residues was inconsistent with the uniform sharpness of resonances for the other peptide protons.

Further evidence in favor of disulfide connectivity between the fourth and fifth cysteines comes from comparison of the inter-residue distances between Cys5α-Cys17β. The NOE cross-peak intensity detected in the three NOESY spectra collected at 700 MHz is inconsistent with the large distance expected for a disulfide bond between the second and fourth cysteines. Additional evidence supporting linkage of the fourth cysteine to fifth cysteine comes from the slowly exchanging amide proton of Phe^4 of hepcidin-20. Inspection of the structures indicates that a possible intramolecular hydrogen bond could only form with the carbonyl oxygen of the first cysteine. The overall energy range calculated for the 20 lowest energy structures independently and in a water box indicates that introduction of the Phe^4 hydrogen bond is consistent with the conformation created in the structure resulting from fourth to fifth disulfide pairing.

These observations indicate that the cysteines link in the following fashion: first to eighth, second to seventh, third to sixth, and fourth to fifth. This arrangement would create a rare vicinal cysteine linkage.

Spectral Assignment and Structure Calculation for Hepcidin-25—Unlike hepcidin-20, inspection of the ^{1}H two-dimensional TOCSY NMR spectra indicated that more amide proton correlations were present in the fingerprint region than could be explained by a single structural conformation (data not shown). Furthermore, some of the correlations appeared somewhat broadened or not clearly resolved. The NOESY data lacked an abundance of backbone amide proton to side chain inter-residue correlations at either 500 or 800 MHz. Clearly, the majority of the correlations in the fingerprint region indicated sequential assignment for Hα_i or Hβ_i to HN$_{(i+1)}$. The bulk of the cross-strand connectivities were assigned from the few remaining correlations. As with hepcidin-20, the hairpin β-sheet structure agreed well with the two-dimensional NOESY correlations observed (Fig. 2*C*).

After assignment of each resonance, a minimum of two conformations emerged with two sets of proton backbone and side chain resonances for residues Thr^2 to Ile^8 inclusive and Cys^{23} to Thr^{25} inclusive. Because this region of the peptide is centered about Pro^5, contributions from proline *cis*- and *trans*-conformations would explain a doubling of these proton resonances.

Similar to the hepcidin-20 spectra acquired at 700 MHz, the dispersion provided by the two-dimensional NOESY acquired at 800 MHz established a strong interaction between the first and eighth Cys α-protons and a slightly weaker interaction between the third and sixth Cys β-protons. Using these linkages to establish two disulfide bridges along with unambiguous constraints from Cys7β-Cys23α, Cys22NH-Cys10α, and Gly12NH-Lys18α, structural annealing calculations were completed. The NOE correlations for the minor conformation were also used to identify residues but were not suitable to calculate the structure of the minor conformational isomer.

As with hepcidin-20, the proton chemical shift index analysis was completed for hepcidin-25 (shown in Fig. 1*D*). The results indicate the presence of β-sheet structure for both sides of the peptide with non-sheet characteristics for the loop.

Structural Evaluation—Results of the ARIA calculations indicate that the 20 lowest energy structures for both hepcidin-20 and hepcidin-25 displayed good root mean square deviation values of 0.696 and 1.68 Å, respectively (Table I). Both of the peptides appear as a β-hairpin with the turn portion of the peptide curled toward the N and C termini (Figs. 2 and 3). The curl in the overall shape of the peptide creates a convex and concave surface on each side of the β-sheet. The degree of curl of the hairpin loop toward the rest of the molecule was the result of a combination of NOE constraints between the protons of adjacent residues as well as the backbone conforming to the constraints introduced by the four disulfide bonds. In the final structures, there were no long-range NOE constraints to establish the degree of curl of the peptide loop. Inspection of the cysteine pairings reveals that the disulfide bridges alternate on each side of the sheet, beginning on the convex side of the molecule at the two termini. Similar pairings have been noted for antimicrobial β-sheet peptides such as tachyplesin (26) and protegrin (9). Following from the N-terminal end, the hairpin

TABLE II
Peptide sizing data indicating oligomer size for hepcidin-20 and -25 peptides

Peptide	Concentration (M × 10^{-3})	Hydrodynamic radius	No. of molecules
Hepcidin-20	0.783	10.8	1
	0.783	10[a]	1
	3.76	9.7	1
Hepcidin-25	0.65	13.2	1–2
	1.07	14.5	2
	1.61	17.6	4
	2.93	27.5	17
	1.78	[b]	7

[a] Dynamic light scattering.
[b] Ultracentrifugation data approximate molecular weight 20,625 at 26,000 rpm.

turn begins at the vicinal cysteine juncture and ends at the arginine residue for both peptides. Further inspection of the side chain distribution shows that the convex side contains the hydrophobic side chains, whereas the concave side has the positively charged side chains, giving the peptide amphipathic characteristics (Fig. 4). These features have been noted to be typical for antimicrobial peptides (27).

Perhaps the most intriguing feature of these two peptides is the vicinal cysteine disulfide bond between the fourth and fifth cysteine residues. Although the fourth cysteine through to the serine residue are all part of the β-hairpin loop, only the proton and ^{13}C resonances of the fourth and fifth Cys resonances are either significantly broadened or unobserved. The intensity of these two cysteines is in sharp contrast to the NOESY correlations for Cys^{10}, Cys^{11}, His^{15}, Arg^{16}, and Ser^{17} that make up the remainder of the loop. This difference in contour appearance for the residues comprising the hairpin portion of the peptides suggests that any flexibility in peptide motion is localized at the fourth and fifth cysteine residues, which are involved in the eight-member vicinal disulfide ring. The presence of the rare vicinal disulfide bridge has been noted in other peptides and proteins. Methanol dehydrogenase (28), insecticidal neurotoxins Janus-faced atracotoxins (29), mercuric reductase (30), and mercuric transport protein (31) contain a vicinal disulfide linkage critical for their activity. For the known structures of methanol dehydrogenase and Janus-faced atracotoxins as well as hepcidin-20 and -25, the vicinal Cys residues are part of a distinct turn that shows the peptide bond between the two Cys residues to reside in a *trans*-configuration. Furthermore, the peptide angles ψ (−53° and −50°) for the fourth Cys and ω (−174° and −171°) and ϕ (−129° and −120° for hepcidin-20 and –25, respectively) of the fifth Cys agree well with values determined for methanol dehydrogenase and Janus-faced atracotoxins (29). The presence of the vicinal disulfide in these compounds has been shown to be critical for enzyme and neurotoxin activity, respectively (25, 32).

NMR Diffusion—The NMR diffusion measurements for hepcidin-20 were carried out at 700 MHz using a comparison of diffusion constants between dioxane and the peptide. The peptide sizing data from NMR diffusion, sedimentation, and dynamic light scattering are shown in Table II. Comparison of the diffusion constants between dioxane and hepcidin-20 along with the hydrodynamic radius indicates that hepcidin-20 is a monomer in solution at the observed concentrations. Therefore, all observed NOE interactions from hepcidin-20 would be intramolecular and should be consistent with a monomeric structure.

The tabulated results indicate that although hepcidin-20 exists as a monomer over the concentration values tested, hepcidin-25 aggregates as the concentration was increased. Sedimentation studies carried out on hepcidin-25 gave unusual results consistent with hepcidin-25 aggregating to the point of precipitation as the spinning speed was increased. The lowest spinning speed used for data collection is indicated in Table II.

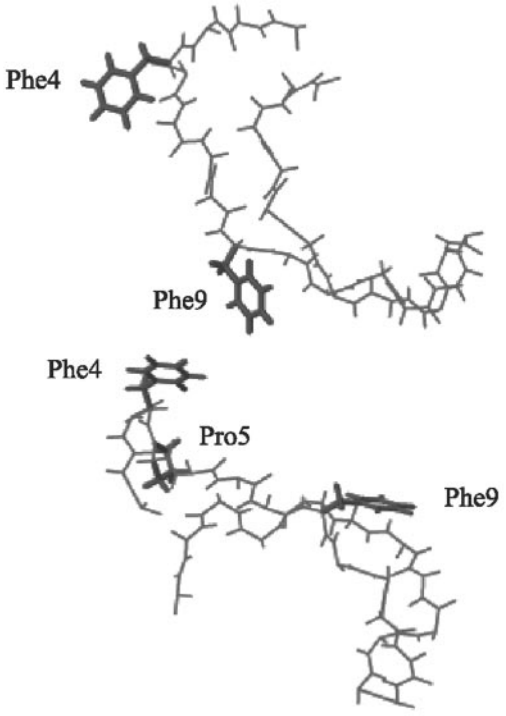

FIG. 5. **Structures indicating possible interactions for aggregate interface.** In this model, Phe^4 would form an intermolecular interaction with Phe^9 of another molecule. This model is supported by extra peaks in the NOESY not assignable to intramolecular interactions.

DLS studies also indicated that a high molecular weight aggregate was present at 1.61 mM (data not shown). Further indication of aggregation properties for hepcidin-25 was noted from a comparison of the NOE buildup curves for hepcidin-20 and -25 (data not shown).

Mode of Aggregation for Hepcidin-25—The presence of additional correlations in the two-dimensional NOESY spectra that could not be assigned to either the major or minor conformations of hepcidin-25 suggests a possible multimer interface between aggregating molecules. Analysis of the NOEs indicates that nine such interactions involved Pro^5 and Phe^4 to Phe^9 and Met^{21} (shown in Fig. 5). The presence of the additional correlations indicates that the formation of multimers occurs in a nonsymmetrical manner, with the main interface occurring between the side chains of Phe^4, Pro^5, Phe^9, and Met^{21}. The loss of the Phe^4 and Pro^5 residues in hepcidin-20 and the concomitant loss of aggregation would also support the multimeric interface involving predominantly the two phenylalanine residues of hepcidin-25. One possible arrangement satisfying these restraints is indicated in Fig. 5. The interfacial region established between Phe^4 and Phe^9 readily permits further aggregation with increasing concentration. The loss of the

first five residues between hepcidin-25 and -20 removes the hydrophobic Pro and Phe and introduces a charged primary amide at Ile[6]. The reduction of hydrophobic character of this portion of the peptide sequence would most likely reduce the propensity to aggregate.

Another feature possibly associated with the aggregation is the difference in appearance between hepcidin-20 and -25 with respect to the proximity of the loop portion of the peptide to the rest of the peptide. In the structure of hepcidin-25, the loop is further away or more open in appearance than that seen with hepcidin-20. This difference in conformation may be caused by the stacking of hepcidin-25 molecules in the aggregate because there were no specific NOE interactions defining the proximity of the loop to the rest of the molecule.

In summary, the structures of hepcidin-20 and -25 reveal a distorted β-sheet shape with a hairpin loop. The β-sheet structure is stabilized by disulfide pairing of Cys residues and hydrogen bonding between the two antiparallel strands. This leads to a markedly amphipathic peptide structure, a hallmark of many antimicrobial and antifungal peptides. The aggregation properties of hepcidin-25 may explain the difference in antimicrobial activity when compared with hepcidin-20. The rare vicinal disulfide pairing in the hairpin loop of hepcidin may be a significant characteristic in the function of this peptide. It would be interesting to explore whether the vicinal Cys bridge is critical to the iron uptake activity of hepcidin.

Acknowledgments—Dr. Brian Tack is gratefully acknowledged for his support in the course of these studies. We acknowledge Peter Y. Shen for his capable assistance. Alan J. Waring performed the peptide syntheses, and Erika V. Valore prepared and supervised the refolding and purification protocol. We appreciate the comments made by Aalim Weljie in the preparation of the manuscript. We thank Dr. Cyril Kay and Les Hicks from the University of Alberta for collection and analysis of the sedimentation data. We also thank the National High Field Nuclear Magnetic Resonance Centre for assistance and use of the facilities. Operation of the National High Field Nuclear Magnetic Resonance Centre is funded by the Canadian Institute for Health Research, Natural Science and Engineering Research Council, and the University of Alberta. H. J. V. and H. N. H thank the Canadian Foundation for Innovation, the Alberta Science and Research Authority, the Alberta Intellectual and Infrastructure Partnership Program, and Alberta Heritage Foundation for Medical Research for financial support in purchasing the 700 MHz spectrometer, Cryo-probe, and upgrades to the 400 and 500 MHz NMR console for the Bio-NMR center in Calgary. The latter facility is supported by maintenance grants provided by the Canadian Institute for Health Research and the University of Calgary.

REFERENCES

1. Park, C. H., Valore, E. V., Waring, A. J., and Ganz, T. (2001) *J. Biol. Chem.* **276,** 7806–7810
2. Krause, A., Neitz, S., Magert, H. J., Schulz, A., Forssmann, W. G., Schulz-Knappe, P., and Adermann, K. (2000) *FEBS Lett.* **480,** 147–150
3. Pigeon, C., Ilyin, G., Courselaud, B., Leroyer, P., Turlin, B., Brissot, P., and Loreal, O. (2001) *J. Biol. Chem.* **276,** 7811–7819
4. Shike, H., Lauth, X., Westerman, M. E., Ostland, V. E., Carlberg, J. M., Van Olst, J. C., Shimizu, C., Bulet, P., and Burns, J. C. (2002) *Eur. J. Biochem.* **269,** 2232–2237
5. Nicolas, G., Bennoun, M., Devaux, I., Beaumont, C., Grandchamp, B., Kahn, A., and Vaulont, S. (2001) *Proc. Natl. Acad. Sci. U. S. A.* **98,** 8780–8785
6. Nicolas, G., Bennoun, M., Porteu, A., Mativet, S., Beaumont, C., Grandchamp, B., Sirito, M., Sawadogo, M., Kahn, A., and Vaulont, S. (2002) *Proc. Natl. Acad. Sci. U. S. A.* **99,** 4596–4601
7. Fleming, R. E., and Sly, W. S. (2001) *Proc. Natl. Acad. Sci. U. S. A.* **98,** 8160–8162
8. Schibli, D. J., Hunter, H. N., Aseyev, V., Starner, T. D., Wiencek, J. M., McCray, P. B., Jr., Tack, B. F., and Vogel, H. J. (2002) *J. Biol. Chem.* **277,** 8279–8289
9. Matsuzaki, K., Nakayama, M., Fukui, M., Otaka, A., Funakoshi, S., Fujii, N., Bessho, K., and Miyajima, K. (1993) *Biochemistry* **32,** 11704–11710
10. Aumelas, A., Mangoni, M., Roumestand, C., Chiche, L., Despaux, E., Grassy, G., Calas, B., and Chavanieu, A. (1996) *Eur. J. Biochem.* **237,** 575–583
11. Berrocal-Lobo, M., Segura, A., Moreno, M., Lopez, G., Garcia-Olmedo, F., and Molina, A. (2002) *Plant Physiol.* **128,** 951–961
12. Hwang, T. L., and Shaka, A. J. (1995) *J. Magn. Reson. A* **112,** 275–279
13. Johnson, B. A., and Blevins, R. A. (1994) *J. Biomol. NMR* **4,** 603–614
14. Wilkins, D. K., Grimshaw, S. B., Receveur, V., Dobson, C. M., Jones, J. A., and Smith, L. J. (1999) *Biochemistry* **38,** 16424–16431
15. Jones, J. A., Wilkins, D. K., Smith, L. J., and Dobson, C. M. (1997) *J. Biomol. NMR* **10,** 199–203
16. Merrill, M. R. (1993) *J. Magn. Reson.* **103,** 223–225
17. Brunger, A. T., Adams, P. D., Clore, G. M., DeLano, W. L., Gros, P., Grosse-Kunstleve, R. W., Jiang, J. S., Kuszewski, J., Nilges, M., Pannu, N. S., Read, R. J., Rice, L. M., Simonson, T., and Warren, G. L. (1998) *Acta Crystallogr. Sect. D Biol. Crystallogr.* **54,** 905–921
18. Nilges, M., and O'Donoghue, S. I. (1998) *Prog. NMR Spect.* **32,** 107–139
19. Koradi, R., Billeter, M., and Wüthrich, K. (1996) *J. Mol. Graphics* **14,** 51–55
20. Nicholls, A., Sharp, K. A., and Honig, B. (1991) *Proteins* **11,** 281–296
21. Laskowski, R. A., MacArthur, M. W., Moss, D. S., and Thornton, J. M. (1993) *J. Appl. Crystallogr.* **26,** 283–291
22. Wishart, D. S., and Sykes, B. D. (1994) *J. Biomol. NMR* **4,** 171–180
23. Wishart, D. S., Sykes, B. D., and Richards, F. M. (1992) *Biochemistry* **31,** 1647–1651
24. Zahn, R., Damberger, F., Ortenzi, C., Luporini, P., and Wüthrich, K. (2001) *J. Mol. Biol.* **313,** 923–931
25. Kao, P. N., and Karlin, A. (1986) *J. Biol. Chem.* **261,** 8085–8088
26. Kawano, K., Yoneya, T., Miyata, T., Yoshikawa, K., Tokunaga, F., Terada, Y., and Iwanaga, S. (1990) *J. Biol. Chem.* **265,** 15365–15367
27. Hwang, P. M., and Vogel, H. J. (1998) *Biochem. Cell Biol.* **76,** 235–246
28. Blake, C. C., Ghosh, M., Harlos, K., Avezoux, A., and Anthony, C. (1994) *Nat. Struct. Biol.* **1,** 102–105
29. Wang, X., Connor, M., Smith, R., Maciejewski, M. W., Howden, M. E., Nicholson, G. M., Christie, M. J., and King, G. F. (2000) *Nat. Struct. Biol.* **7,** 505–513
30. Moore, M. J., Miller, S. M., and Walsh, C. T. (1992) *Biochemistry* **31,** 1677–1685
31. Morby, A. P., Hobman, J. L., and Brown, N. L. (1995) *Mol. Microbiol.* **17,** 25–35
32. Park, C., and Raines, R. T. (2001) *Protein Eng.* **14,** 939–942